Tunneling Aharonov-Bohm interferometer on helical edge states

R. A. Niyazov,[1,2] D. N. Aristov,[1,3,4] and V. Yu. Kachorovskii[5,2,3]

[1] *NRC "Kurchatov Institute", Petersburg Nuclear Physics Institute, Gatchina 188300, Russia*
[2] *L. D. Landau Institute for Theoretical Physics,142432, Moscow Region, Chernogolovka, Russia*
[3] *Institut für Nanotechnologie, Karlsruhe Institute of Technology, 76021 Karlsruhe, Germany*
[4] *St.Petersburg State University, 7/9 Universitetskaya nab., 199034 St. Petersburg, Russia*
[5] *A. F. Ioffe Physico-Technical Institute, 194021 St. Petersburg, Russia*

(Dated: September 3, 2022)

We discuss transport through an interferometer formed by helical edge states tunnel-coupled to metallic leads. We focus on the experimentally relevant case of relatively high temperature as compared to the level spacing and discuss a response of the setup to the external magnetic flux ϕ (measured in units of flux quantum) piercing the area encompassed by the edge states. We demonstrate that tunneling conductance of the interferometer is structureless in ballistic case but shows sharp antiresonances, as a function of magnetic flux ϕ — with the period 1/2— in the presence of magnetic impurity. We interpret the resonance behavior as a coherent enhancement of backward scattering off magnetic impurity at integer and half-integer values of flux, which is accompanied by suppression of the effective scattering at other values of flux. Both enhancement and suppression are due to the interference of processes with multiple returns to magnetic impurity after a number of clockwise and counterclockwise revolutions around setup. This phenomenon is similar to the well-known weak-localization-induced enhancement of backscattering in disordered systems. The quantum correction to the tunneling conductance is shown to be proportional to flux-dependent "ballistic Cooperon". The obtained results can be used for flux-tunable control of the magnetic disorder in Aharonov-Bohm interferometers built on helical edge states.

PACS numbers:

arXiv:1804.01115v2 [cond-mat.mes-hall] 26 Apr 2018

I. INTRODUCTION

The quantum interferometry is a rapidly growing area of fundamental research with a huge potential for applications in optics, electronics, and spintronics. One of the simplest realization of quantum electronic interferometer is a ring-geometry setup tunnel-coupled to metallic leads. Such a device can be controlled by magnetic field due to the Aharonov-Bohm (AB) effect [1, 2]. The AB interferometers formed by single or few ballistic quantum channels are very attractive both from a fundamental point of view as prime devices to probe quantum coherent phenomena and in view of possible applications as miniature and very sensitive sensors of magnetic field (we present a brief review of publications on this topic in the next section). Although they have been studied in detail theoretically, their practical implementation faces significant difficulties. The complexity of creating of ballistic single- or few-channel interferometers based on conventional semiconductors, such as GaAs or Si, is connected with technological problems of manufacturing one-dimensional clean systems. The efficiency of quantum electronic interferometers used in practice is limited by rather stringent requirements, for example, very low temperature for interferometers based on superconducting SQUIDs or the requirement of very strong magnetic fields for interferometers based on the edge states of the Quantum Hall Effect systems.

A promising opportunity for a technological breakthrough in this direction is associated with the discovery of topological insulators, which are materials insulating in the bulk, but exhibiting conducting channels at the surface or at the boundaries. In particular, the two-dimensional topological insulator phase was predicted in HgTe quantum wells [3–5] and confirmed by direct measurements of conductance of the edge states [6] and by the experimental analysis of the non-local transport [7–10]. These states are one-dimensional helical channels where the electron spin projection is connected with its velocity, e.g. electrons traveling in one direction are characterized by spin "up", while electrons moving in the opposite direction are characterized by spin "down". Remarkably, the electron transport via helical edge states is ideal, in the sense that electrons do not experience backscattering from conventional non-magnetic impurities, similarly to what occurs in edge states of Quantum Hall Effect systems, but without invoking high magnetic fields (for detailed discussion of properties of helical edge states see Refs. [11, 12]). Hence, in the absence of magnetic disorder, the boundary states are ballistic and the intereferometers constructed on such states are topologically protected from external perturbations. Due to this key advantage the helical edge states are very promising candidates for building blocks in quantum spin-sensitive interferometry.

The topological insulators has become a hot topic in the last decade (see Refs. [13–27] and references therein). Particularly, different manifestations of the AB effect in topological insulators were discussed: the dependence of the longitudinal conductance of nanoribbons and nanowires on the magnetic flux piercing their cross-section was studied [16, 26]; weak antilocalization was investigated in the disordered topolgical insulators and oscillations with magnetic flux with the period equal to the

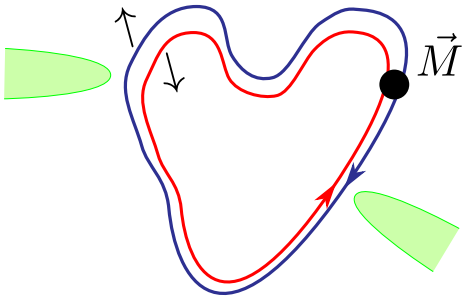

FIG. 1: Ring-shape interferometer formed by helical edge states tunnel-coupled to the metallic point contacts. The upper shoulder of the interferometer contains magnetic impurity which serves as a backscattering center.

half of the flux quantum were predicted [15, 20]. The AB effect was also discussed for almost closed loops formed by curved edge states [18]. Experimentally, the AB oscillations were observed in the magnetotransport measurements of transport (both local and nonlocal) in 2D topological insulators based on HgTe quantum wells [28] and were explained by coupling of helical edges to bulk puddles of charged carriers.

The purpose of the current paper is to discuss standard AB setup (see Fig. 1) focusing on the effect of the magnetic impurities. We consider an interferometer formed by helical-edge states of a 2D topological insulator tunnel-coupled to leads. We assume that upper and lower shoulders of interferometer have, respectively, lengths L_1 and L_2. We limit ourselves to discussion of setup with a single impurity placed into upper shoulder at the distance s (along the edge) from the left contact. This case captures all essential physics of the problem and can be easily generalized for a more general case of arbitrary number of magnetic centers provided that magnetic disorder is weak and the corresponding localization length is large compared to interferometer circumference $L = L_1 + L_2$.

Such AB interferometer built on the helical edge states was studied theoretically at zero temperature [13, 19, 24]. It is known, however, that the form and shape of the AB oscillations strongly depend on the relation between temperature T and level spacing Δ connected with the finite size of the system (see Sec. II). In our case, $\Delta = 2\pi v_F/L$ is controlled by total length L. For typical sample parameters, $L = 10$ μm, and $v_F = 10^7$ cm/s, we estimate the level spacing $\Delta \approx 3$ K. Having in mind not too low temperatures, we focus on the experimentally relevant case,

$$T \gg \Delta, \tag{1}$$

and discuss dependence of the tunneling conductance G of the setup on the external magnetic flux Φ piercing the area encompassed by edge states. Simple estimates show that the flux quantum, $\Phi_0 = hc/e$, is achieved for rings of the above size in fields $B \sim 3$ Oe, well below the expected magnitude of the fields destroying the edge states [29–31]. Therefore, in what follows, we neglect the influence of the magnetic fields on the helical states. We will demonstrate the existence of interference-induced effects, which are robust to the temperature, i.e. survive under condition (1), and can therefore be obtained for relaxed experimental conditions. Specifically, we find that G is structureless in ballistic case but shows a sharp antiresonances, as a function of $\phi = \Phi/\Phi_0$ in the presence of magnetic impurities. Although similar antiresonances are known to arise in the single-channel rings made of conventional materials (see review of the relevant references in the next section), the helical AB interferometer shows essentially different behavior due to specific properties of the edge states. Most importantly, the effect is more universal and robust to details of the setup, in particular, to relation between L_1 and L_2. Another difference concerns the periodicity of the function $G(\phi)$, which — for the case of helical edge state interferometer — obeys

$$G(\phi + 1/2) = G(\phi),$$

while for interferometers made of conventional materials, this function is periodic with the period 1.

We interpret the resonance behavior of conductance as a coherent enhancement of backward scattering off magnetic impurities at certain values of ϕ. The effect arises due to interference contribution from trajectories containing multiple returns to magnetic impurity after ballistic revolutions around the setup in clockwise and counterclockwise directions. Such processes are specific for closed geometry of the system and are absent in the infinite helical edge containing backscattering centers (see discussion of transport in latter system in a number of recent publications [32–42]). We notice, however, that bulk puddles of charged particles coupled to infinite helical edge [35, 36, 41] (or curved edge states with tunneling coupling between different points [18, 34]) can serve as mini-resonators and the edge transport can probe levels in these resonators. This effect was used for interpretation of experimental results on AB oscillations in nonlocal transport measurements in HgTe quantum well [28]. What we claim here is that for almost closed AB interferometer with very weak tunneling coupling to the leads, the circumference of the interferometer itself can serve as such a resonator and increase or decrease — depending on the value of ϕ — scattering on the impurity.

Return trajectories corresponding to propagation in opposite directions with equal winding numbers give flux-sensitive contribution to interference part of the conductance. Hence, the effect is somewhat similar to the weak-localization-induced enhancement of backscattering caused by multiple diffusive returns to impurity in a disordered system. The only essential difference in the case under discussion is that the returns to impurity are ballistic. We show below that the coherent enhancement of backscattering occurs at integer and half-integer values of ϕ and is accompanied by suppression of backscattering (or, equivalently, enhancement of forward scattering) at other values of ϕ. As a result, the tunneling conduc-

tance shows sharp antiresonances separated by the distance $\Delta\phi = 1/2$. It is worth noting that the coherent backscattering can occur even in the absence of magnetic impurities provided that the edge states are curved so that some points at the edge are close to each other and can serve as backscattering centers due to tunneling coupling [18].

A very sharp dependence of the conductance on magnetic field opens a wide avenue for applications in the area of extremely sensitive detectors of magnetic fields. Most importantly, the predicted dependence of effective scattering probability on the magnetic flux, allows one to manipulate magnetic disorder by external field.

II. AHARONOV-BOHM INTERFEROMETERS MADE OF CONVENTIONAL MATERIALS

In this Section, we present a brief review of properties of the AB interferometers formed by conventional (non-helical) *single- or few-channel ballistic* channels, which were actively studied in last decades [43–72].

For noninteracting ring, the tunneling conductance of the interferometer,

$$G = N\frac{e^2}{h}\mathcal{T}\,, \tag{2}$$

is expressed in terms of energy-averaged tunneling transmission coefficient $\mathcal{T} = -\int d\epsilon\, \mathcal{T}(\epsilon)\partial_\epsilon f_F(\epsilon)$, where f_F is the Fermi distribution function and N is the number of the conducting channels. The tunneling conductance is known to exhibit different types of oscillations. Specifically, $\mathcal{T}(\epsilon)$ oscillates as a function of energy of the tunneling electron ϵ, having maxima at positions of quantum levels in the ring [43–45]. For low temperatures, $T \ll \Delta$, these oscillations transform into oscillations of G with the Fermi energy, which are strongly affected by the Coulomb blockade in the interacting case [52]. In the opposite high temperature case, $T \gg \Delta$, these oscillations are exponentially suppressed.

Magnetic field applied to the ring leads to another type of oscillations —periodic oscillation of G with the dimensionless magnetic flux ϕ piercing the area encompassed by quantum channels. The period of the oscillations is given by the flux quantum $\Delta\phi = 1$. The oscillations arise due to interference of electron trajectories winding around the ring and represent a nice manifestation of the Aharonov-Bohm effect [1, 2]. The shape and amplitude of the oscillations depend essentially on the strength of the tunneling coupling and on the relation between T and Δ. For $T \ll \Delta$ and weak tunneling coupling there are narrow resonant peaks in the dependence $G(\Phi)$ [43–45]. The positions of the peaks depend on the electron Fermi energy [43] and on the strength of the electron-electron interaction [52]. Remarkably, the interference effects are not entirely suppressed with increasing the temperature, and the resonant behavior of $G(\Phi)$ survives for the case $T \gg \Delta$. Specifically, the high-temperature conductance of the noninteracting ring weakly coupled to the contacts exhibits sharp antiresonances at $\phi = 1/2+n$, where n is an arbitrary integer number [46, 68]. The antiresonances are broadened by weak disorder [70]. The electron-electron interaction leads to appearance of a fine structure of the antiresonances: each antiresonance splits into a series of narrow peaks, whose widths are governed by dephasing [68, 71]. Spin-charge separation in the interacting spinful interferometer leads to the additional splitting of antiresonances because of existence of two types of excitations (charge and spin excitations) proparating with different velocities [46, 72].

Additional physics comes into play in the presence of the spin-orbit (SO) interaction, which results in a phase acquired by the spin part of the electron wave propagating around the ring. This phase is added to AB phase and leads to the third type of the conductance oscillations: periodic oscillations of G with the strength of the SO coupling, so called Aharonov-Casher (AC) effect [73–75]. The effect of SO on the performance of the AB interferometer was intensively discussed [73–95] with the focus on zero-temperature case. The finite temperature effects were also analyzed both numerically [80, 84, 89], and analytically [96]. In particular, it was found in Ref. [96] that AC effect is also robust to temperature: for $T \gg \Delta$, the antiresonances in the conductance are split by SO coupling with the splitting distance proportional to the AC phase.

Importantly, the antiresonances arising in the usual AB interferometers at high temperatures, $T \gg \Delta$, turn out to be very sensitive to the geometry of the problem [68, 70–72, 96]. In particular, their shape and width are strongly modified for interferometer with non-equal shoulders, $L_1 \neq L_2$ [97]. As we will see, this is not the case for interferometer formed by helical edge states. In the latter case, the antiresonances are not sensitive to geometry of the device: their amplitude and width do not depend on the relative lengths of the interferometer shoulders and on the position of the magnetic impurity. Also they do not change in the non-planar geometry of the sample. Physically, this happens because multiple returns to magnetic impurity—the effect responsible for coherent enhancement of magnetic disorder—are only sensitive to the total length of the edge and robust to other details of the interferometer, e.g., to relation between L_1 and L_2.

In order to clarify this point in more detail, we note that there are two key physical difference between conventional interferometer and one built on helical edge states. First is the absence of backscattering by non-magnetic contacts in the case of helical edge channels. The backscattering destroys antiresonances in the symmetrical setup ($L_1 = L_2$) at integer values of magnetic flux and restores the periodicity of the conductance with the period $\Delta\phi = 1$ in the conventional single-channel interferometers, both ballistic [68, 97] and containing impurities [70]. In the asymmetrical setup ($L_1 \neq L_2$), the antiresonances at $\phi = n$ exist but they have different

widths and amplitudes as compared to antiresonances at $\phi = n + 1/2$ [97]. For helical-edge case, where backscattering is prohibited, the antiresonances at $\phi = n$ and $\phi = n + 1/2$ are identical, hence, periodicity of tunneling conductance takes place with $\Delta\phi = 1/2$. Second difference concerns the Berry's phase containing the whole information about the details of the structure of the helical edge states. As is discussed below, for helical edge states this geometrical phase simply redefines the dynamical phase and drops out after thermal averaging in contrast to conventional interferometers, where Berry phase determines splitting of antiresonsnces [96].

III. BASIC EQUATIONS

We consider the setup depicted in Fig. 1. The helical edge states of two-dimensional topological insulator are tunnel-coupled to metallic nonmagnetic point contacts. Spin and momentum are locked in the helical state: electrons with different spin projections propagate in opposite directions. We model metallic contacts by single-channel spinful wires, so that electrons are injected into the helical states through so-called tunnel Y junctions. We assume that the electrons in the metallic leads are not polarized. The system is pierced by magnetic flux Φ. In this paper we focus on the calculation of the tunneling conductance of the interferometer, whereas interesting effects related to spin-selective properties of the system such as resonance rotation of initial spin polarization will be discussed elsewhere [98].

Since we consider nonmagnetic leads, the different spin projections do not mix at the contacts. Thus, the point contact is described by the time-reversal S-matrix:

$$S = \begin{pmatrix} -t & r & 0 & 0 \\ r & t & 0 & 0 \\ 0 & 0 & -t & r \\ 0 & 0 & r & t \end{pmatrix}. \tag{3}$$

This S-matrix connects incoming states $(l_\uparrow, h_\uparrow, l_\downarrow, h_\downarrow)$ with outgoing states $(l'_\uparrow, h'_\uparrow, l'_\downarrow, h'_\downarrow)$ (see Fig. 2). "l" stands for the leads, "h" stands for the helical edge. This notation corresponds to one in Ref. [99] after obvious rearrangement of channels. The main difference between the Fig. 2a and Fig. 2b is the opposite propagation of electrons with different spins in the helical edge. The tunneling contact is characterized by two amplitudes r and t, obeying $|t|^2 + |r|^2 = 1$. Without a loss of generality, we assume that t and r are real and express them through the parameter γ,

$$r = \frac{2\sqrt{\gamma}}{1+\gamma}, \quad t = \frac{1-\gamma}{1+\gamma}. \tag{4}$$

which has a physical meaning of tunneling transparency of the contact [68, 71, 100].

We calculate below the transmission coefficient by direct summation of the amplitudes corresponding to clockwise and counterclockwise propagating trajectories with different winding numbers.

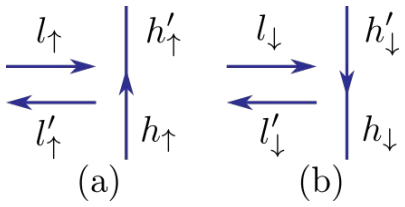

FIG. 2: Point contact between the helical ring and the spinful wire.

		chirality	
		+	−
spin	↑	$\boldsymbol{kL + \phi + \delta}$	$kL - \phi - \delta$
	↓	$kL + \phi - \delta$	$\boldsymbol{kL - \phi + \delta}$

TABLE I: Phases of electron wave function after a full revolution in the arbitrary setup shown in Fig. 1.

Let us calculate the phase acquired by the electron wave after a full revolution around setup shown in Fig. 1. In order to make the physical picture more transparent, we consider first a general case with two chiralities (direction of propagation) and two spins not necessarily aligned with momentum (this case corresponds to a conventional single-channel spinful wire). The acquired phase includes three terms: a dynamical contribution kL (here k is the electron wave vector), magnetic phase $\pm 2\pi\phi$ and the Berry phase $\pm\delta$ [101], given by one half of the solid angle, subtended by spin direction during circumference of the interferometer. The dynamical contribution depends on L only and does not change its sign when changing the chirality and spin projection. By contrast, the sign of magnetic phase is insensitive to spin but changes sign with changing the chirality. The Berry's phase changes sign both with changing the chirality and with changing the spin (see Tab. I). For helical edge only two electron states from the Table I are present, which are marked in boldface in Table I. All information about the structure of the edge states, curvature of the interferometer etc., is encoded in the Berry's phase, but as we see, it can be fully incorporated into dynamical phase kL. This should be contrasted to the case for conventional interferometers with weak SO coupling, where Berry's phase contributes to the Aharonov-Casher phase (see discussion in Ref. [96]).

IV. CONDUCTANCE CALCULATION

In this Section we calculate the tunneling conductance of the setup, which is given by Eq. (2) with $N = 2$. We have $G = (2e^2/h)\mathcal{T}$, where, for the case of spin-unpolarized contacts, the transmission coefficient can be represented as an average over incoming spin polariza-

tions

$$\mathcal{T} = \frac{\mathcal{T}_\uparrow + \mathcal{T}_\downarrow}{2}\,. \tag{5}$$

For fully ballistic interferometer, $\mathcal{T}$ does not contain interference term and hence is flux-independent. Indeed, the right- and left- moving electrons have opposite spin projections at any point, in particular at the point contact where they exit the ring. Consequently, they can not interfere in the tunneling process. Next, we use the condition (1), which means that the variation of the electron wave vector within the temperature window, δk, is large, $\delta k\, L \gg 1$. Due to this inequality, interference contribution coming from any two trajectories of the same chirality and with different winding numbers n and m becomes exponentially small, $\propto \exp(-\delta k L|n-m|)$, after the thermal averaging. Neglecting such exponentially small terms, we arrive at the conclusion that only trajectories with the same chirality and $n = m$ contribute. In other words, the transmission coefficient is given by purely classical contributions, while all the interference terms are suppressed. Classical contribution from the trajectory with certain chirality and winding number n to the transmission coefficient is given by $\left|r \cdot t^{2n} \cdot r\right|^2$, The summation over n yields $\mathcal{T}_\uparrow = \mathcal{T}_\downarrow = r^4/(1-t^4)$, and the use of (4) leads to

$$\mathcal{T} = \frac{2\gamma}{1+\gamma^2}. \tag{6}$$

Here the case $\gamma \ll 1$ corresponds to weak tunnel coupling mostly considered in this paper, and fully open setup is described by $\gamma = 1$. A more general expression for the classical part of the conductance in the presense of magnetic impurity will be derived below [see Eq. (25)].

Let us now demonstrate that the magnetic impurities induce quantum interference corrections to the conductance. This feature is of crucial importance for applications, since it allows to measure a degree of magnetic disorder by changing the magnetic flux piercing the ring. For simplicity, we restrict ourselves to the analysis of the AB helical-states interferometer having a single magnetic impurity in one of its shoulders. This case is easily solvable and captures the basic physics of the problem. A generalization to more complicated setups with many magnetic scatterers is much more involved but should not lead to essential modifications of the results provided that magnetic disorder is weak, so that L is much smaller than the corresponding localization length.

Physically, the quantum correction to conductance appears due to interference contribution coming from the trajectories containing multiple returns to the magnetic impurity. To clarify this point, let us consider two processes shown in Fig. 3 a, b corresponding to the tunneling of electron with the initial spin $|\uparrow\rangle$ [we will call these processes as (a) and (b), respectively]. The process (a) does not involve backscattering by magnetic impurity, while the process (b) includes two backscattering acts. We see that the final spin states coincide, so that these

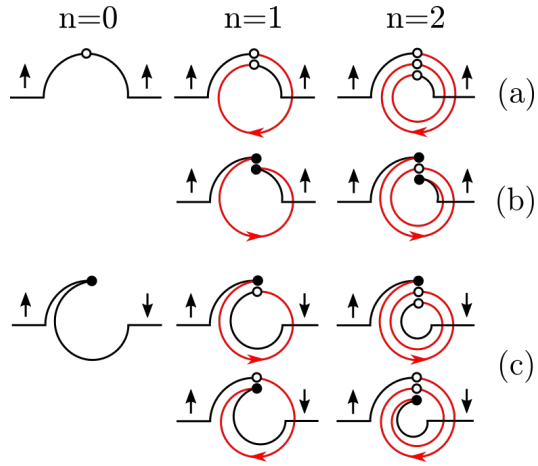

FIG. 3: Processes with incoming spin up projection, involving ballistic propagator as well as single and double backscattering processes at the magnetic impurity. Backscattering events with the corresponding amplitude $i \sin\theta$ are marked by black dots. Forward scattering events by the magnetic impurity are shown by open circles and has amplitude $\cos\theta$. The processes (a) and (b) with coinciding initial and final polarization can interfere. The process (c) corresponds to spin-flip tunneling process. A number of returns to the magnetic impurity denoted by n. The processes shown in (a) and (b) with equal n correspond to n revolutions around the ring in opposite directions.

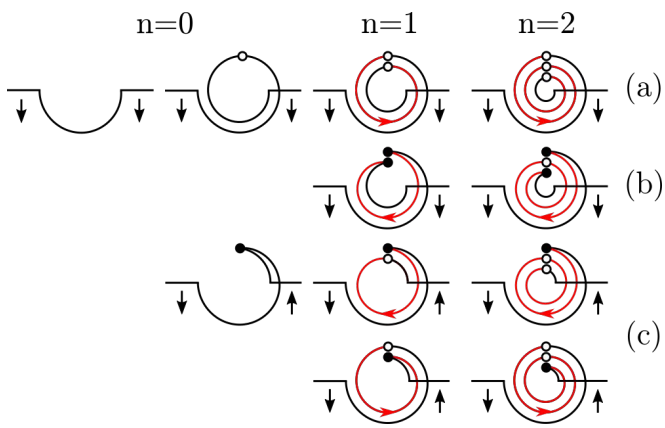

FIG. 4: The same as in Fig. 3 but with spin down projection.

processes can interfere. Both processes include full revolutions around the setup, and we thus should sum over the number n of returns to magnetic impurity (winding number). For equal winding numbers, trajectories (a) and (b) have the same lengths and therefore lead to a contribution to the interference part of the conductance, which survives after the thermal averaging. Indeed, trajectories (a) and (b) with equal n contain a loop (marked by red color in Figs. 3a,b) where both trajectories start from magnetic impurity and make n full revolutions in the opposite directions, clockwise for the trajectory (a) and counterclockwise for the trajectory (b). Hence, the contribution to the interference part of the conductance

coming from these two processes is flux-dependent. We notice, that such interference contribution is very similar to the quantum correction to the conductivity of disordered system caused by weak localization phenomenon. The only essential difference is that in the disordered systems the closed interference loops are formed by diffusive trajectories, while in the case of helical edges the effect arises due to ballistic returns to the magnetic impurity.

The spin-flip tunneling processes also contribute to the interference correction to the conductance. Such processes containing single backscattering act are shown in Fig. 3c. As illustrated in this figure, two spin-flip processes with a given winding number but different sequence of backward and forward scattering events can contain a closed loop (marked by red color) passed in the opposite directions. Since such processes have equal lengths and the same final spins, they can interfere and the corresponding flux-sensitive interference contribution is not affected by the thermal averaging.

We stress that the flux-dependent terms in the tunneling conductance appear solely due to the presence of the magnetic impurity. In the rest of this section we focus on the direct calculation of interference contribution to the conductance. A physical interpretation is given in more detail in Sec. V. We demonstrate there, that all quantum corrections to the conductance can be taken into account by simple renormalization of the backscattering probability by magnetic impurity.

Let us calculate the tunneling transmission coefficient through the interferometer assuming that the magnetic impurity is described by the scattering matrix of general form

$$\hat{S}_M = \begin{pmatrix} \cos\theta & i\sin\theta\ e^{i\varphi} \\ i\sin\theta\ e^{-i\varphi} & \cos\theta \end{pmatrix}. \tag{7}$$

We will discuss the case of classical impurity with large magnetic moment $\mathbf{M}$ ($M \gg 1$). Then, in the first approximation, one can neglect feedback effect related to the dynamics of $\mathbf{M}$ caused by exchange interaction with the ensemble of right- and left-moving electrons (for infinite helical edge, this effect was discussed in Refs. [42]). In this section, we assume that impurity is static and elements of matrix $\hat{S}_M$ do not change in time. For such impurity, without a loss of generality, one can put $\varphi = 0$. The effects caused by slow random evolution of $\mathbf{M}$ in the external magnetic bath will be briefly discussed in Sec. VI.

We calculate now the conductance perturbatively, assuming that $\theta \ll 1$ and keeping the corrections up to second order, θ^2, to the conductance. (The analysis of general non-perturbative case is more involved and delegated to Appendix B.) Within this approximation one can consider only the ballistic processes and processes with one and two backscattering events. Then, the transmission coefficient for spin $|\uparrow\rangle$ is given by

$$\mathcal{T}_\uparrow = \left\langle \left| A_\uparrow^{(a)} + A_\uparrow^{(b)} \right|^2 + \left| A_\uparrow^{(c)} \right|^2 \right\rangle_\varepsilon . \tag{8}$$

Here index (a) corresponds to processes without backscattering (Fig. 3a), (b) to processes with two backscattering events (Fig. 3b) and (c) to spin-flip processes with a single backscattering act (Fig. 3c) ; thermal averaging is denoted by $\langle \ldots \rangle_\varepsilon$.

The tunneling amplitudes of trajectories shown in Fig. 3a,b are given, respectively, by the following equations

$$\begin{aligned} A_\uparrow^{(a)} &= \frac{r^2 \cos\theta e^{i\varphi_+ L_1/L}}{1 - t^2\cos\theta e^{i\varphi_+}}, \\ A_\uparrow^{(b)} &= \frac{r^2 t^2 (i\sin\theta)^2 e^{i(\varphi_- + \varphi_+ L_1/L)}}{[1 - t^2\cos\theta e^{i\varphi_+}]^2 [1 - t^2\cos\theta e^{i\varphi_-}]}, \end{aligned} \tag{9}$$

which are obtained by direct summation of tunneling amplitudes with different winding numbers. Here

$$\varphi_\pm = kL \pm 2\pi\phi \tag{10}$$

and we incorporated the Berry phase into the dynamical phase. The factor $[1 - t^2\cos\theta e^{i\varphi_+}]^{-1}$ in $A_\uparrow^{(a)}$ appears due to summation of contributions of clockwise rotating ballistic trajectories over winding number n. The denominator in $A_\uparrow^{(b)}$ stems from contributions of clockwise processes with different winding numbers both before and after backscattering, together with contributions of counterclockwise scattering processes between two backscattering acts.

The amplitude of the process shown in Fig. 3c reads

$$A_\uparrow^{(c)} = \frac{r^2 t (i\sin\theta) e^{i[\varphi_+ s/L\ +\ \varphi_-(L+s-L_1)/L]}}{[1 - t^2\cos\theta e^{i\varphi_+}][1 - t^2\cos\theta e^{i\varphi_-}]}, \tag{11}$$

where s is the distance from the left contact to the impurity position.

The processes with opposite incoming spin are shown in Fig. 4. Their contribution reads

$$\mathcal{T}_\downarrow = \left\langle \left| A_\downarrow^{(a)} + A_\downarrow^{(b)} \right|^2 + \left| A_\downarrow^{(c)} \right|^2 \right\rangle_\varepsilon . \tag{12}$$

Again, there are two interfering processes when the outgoing spin polarization is parallel to the incoming one, shown in Fig. 4a,b, and a decoupled process, Fig. 4c. in which initial and final spin polarization are antiparallel. Notice that both $\mathcal{T}_\uparrow$ and $\mathcal{T}_\downarrow$ depend on position of impurity and $\mathcal{T}_\uparrow \neq \mathcal{T}_\downarrow$. Analytical expressions for amplitudes corresponding to the processes in Fig. 4 read

$$\begin{aligned} A_\downarrow^{(a)} &= \frac{r^2 e^{i\varphi_-(L-L_1)/L}}{1 - t^2\cos\theta e^{i\varphi_-}}, \\ A_\downarrow^{(b)} &= \frac{r^2 t^4 (i\sin\theta)^2 e^{i(\varphi_+ + \varphi_-(2L-L_1)/L)}}{[1 - t^2\cos\theta e^{i\varphi_-}]^2 [1 - t^2\cos\theta e^{i\varphi_+}]}, \\ A_\downarrow^{(c)} &= \frac{r^2 t (i\sin\theta) e^{i[\varphi_+(L_1-s)/L + \varphi_-(L-s)/L]}}{[1 - t^2\cos\theta e^{i\varphi_+}][1 - t^2\cos\theta e^{i\varphi_-}]}, \end{aligned} \tag{13}$$

Combining Eqs. (5), (9), (11) – (12), performing energy averaging under the condition (1) with the use of auxiliary formulas given in Appendix A, and expanding results

over θ up to the second order, we find after some algebra

$$\mathcal{T} = \frac{2\gamma}{1+\gamma^2} - \frac{16\gamma^3 A_\gamma\, \theta^2}{1-\cos(4\pi\phi)+32\gamma^2 B_\gamma}. \tag{14}$$

Here we expressed tunneling amplitudes r and t in terms of γ [see Eq. (4)] and introduced coefficients

$$A_\gamma = \frac{1+6\gamma^2+\gamma^4}{(1+\gamma^2)(1-\gamma^2)^4},\ B_\gamma = \frac{(1+\gamma^2)^2}{(1-\gamma^2)^4}, \tag{15}$$

which both depend solely on the tunneling transparency. Equation (14) gives the transmission coefficient for arbitrary tunneling coupling to the leads and weak coupling to magnetic impurity. The latter is taken into account perturbatively. We see that impurity induces dependence of $\mathcal{T}$ on the flux.

Let us consider the limiting cases of Eq. (14). The strong tunneling coupling (almost open ring with $r \to 1$, $t \to 0$) corresponds to $\gamma \to 1$, see Eq. (4). From Eq. (14) we see that the dependence on magnetic flux in this case is very weak:

$$\mathcal{T} \approx 1 - \delta\mathcal{T} - \theta^2 t^4 \cos(4\pi\phi), \qquad \text{for} \quad t \to 0. \tag{16}$$

where we defined the flux-independent correction to the transmission coefficient as $\delta\mathcal{T} \approx \theta^2/2 + 2t^2(1-\theta^2) - (2-4\theta^2)t^4$, and we keep terms up to the order $t^4 \propto (1-\gamma)^4 \ll 1$ in this expansion. Hence, for strong tunneling coupling the magnetic impurity leads to a small correction smoothly dependent on ϕ. This dependence is similar to harmonic dependence on the AB phase predicted in Ref. [34] for $T = 0$ and slightly different geometry of the setup.

By contrast, in the opposite case of almost closed ring weakly coupled to the leads, i.e. $\gamma \to 0$, the dependence on the flux is very sharp:

$$\mathcal{T} \approx 2\gamma \left[1 - \frac{8\gamma^2\theta^2}{1-\cos(4\pi\phi)+32\gamma^2}\right], \quad \text{for} \quad \gamma \to 0. \tag{17}$$

We see that $\mathcal{T}$ shows narrow antiresonances as a function of ϕ of width $\sim \gamma$ at $\phi = n$ and $\phi = n+1/2$. This behavior is different from the behavior of tunneling conductance of a conventional (non-helical) single-channel ring, where antiresonances occur only at $\phi = n + 1/2$ both in clean [68, 71] and disordered case [70]. The key difference is the absence of backscattering on the contacts in the interferometer formed by the helical states.

Equation (17) is obtained within the perturbative calculation with respect to magnetic impurity and includes the first order terms in θ^2. This equation is valid for $\theta \ll \max(\delta\phi, \gamma)$, where $\delta\phi$ is the deviation of flux from the resonance value [$\delta\phi = \phi - n$ or $\delta\phi = \phi - (n+1/2)$]. In Appendix B we present a more rigorous calculation, assuming only that $\gamma \ll 1$, $\theta \ll 1$, and $\delta\phi \ll 1$, and arbitrary relation between $\delta\phi, \gamma$ and θ. The result is given by

$$\mathcal{T} \approx 2\gamma \left[1 - \frac{\theta^2}{4}\frac{\gamma^2}{\gamma^2 + (\pi\delta\phi/2)^2 + (\theta/4)^2}\right]. \tag{18}$$

Thus, the magnetic impurity leads to sharp antiresonances in the dependence of the tunneling conductance on the magnetic flux. Non-perturbative effects lead to appearance of the additional contribution $\theta^2/16$ in the denominator of the resonant term in (18). Physically, this corresponds to the broadening of the antiresonances because of multiple coherent scattering events.

We see that the transmission coefficient and the conductance, $G = G(\phi)$, has minima at $\phi = n/2$, and maxima at $\phi = 1/4 + n/2$ with integer n. Instead of $G(\phi)$ it is convenient to introduce the following normalized function

$$g(\phi) = \frac{G(\phi) - G(0)}{G(1/4) - G(0)}. \tag{19}$$

which is plotted in Fig. 5.

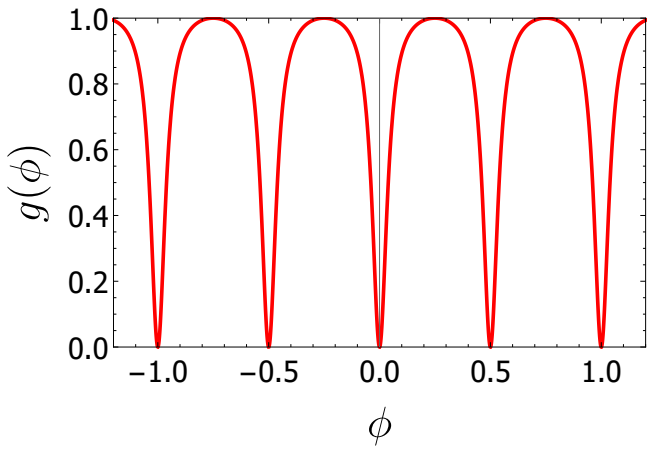

FIG. 5: The sharp antiresonances in the normalized conductance $g(\phi)$, Eq. (19).

V. PHYSICAL INTERPRETATION: COHERENT ENHANCEMENT OF THE SCATTERING OFF MAGNETIC IMPURITY

In this Section we demonstrate that the obtained result can be interpreted in terms of coherent enhancement of backward scattering by magnetic impurity at integer and half-integer values of ϕ, which is accompanied by a decrease of backward scattering (or, equivalently, increase of the forward scattering) at other values of the flux. We will show that the effect is analogous to coherent enhancement of backscattering caused by weak localization (see Ref. [102] for review). As was shown in Ref. [103], the effect of weak localization in 2D electron gas can be fully incorporated into the renormalization of the classical differential cross-section $\Sigma(\theta)$ on a single impurity. The resonant enhancement of backscattering, $\delta\Sigma_{\rm a}(\theta) = \delta\Sigma_{\rm tr}\delta(\theta - \pi)$, is always accompanied by

the angle-independent (in diffusion approximation) decrease of the scattering at other angles, so called non-backscattering contribution, $\delta\Sigma_{\rm b}(\theta) = -\delta\Sigma_{\rm tr}/2\pi$, so that

$$\int d\theta \left[\delta\Sigma_{\rm a}(\theta) + \delta\Sigma_{\rm b}(\theta)\right] = 0.$$

Here $\delta\Sigma_{\rm tr}$ is weak-localization-induced correction to transport scattering cross-section

$$\delta\Sigma_{\rm tr} = \int d\theta \left[\delta\Sigma_{\rm a}(\theta) + \delta\Sigma_{\rm b}(\theta)\right](1-\cos\theta), \qquad (20)$$

which directly contributes to quantum conductivity correction. This correction is proportional to the return probability and, for 2D system, logarithmically diverges with the system size L (for zero temperature and magnetic field): $\delta\Sigma_{\rm tr} \propto \ln L$. On the technical level, this correction is given by a sum of maximally crossed diagrams (the Cooperon). Hence, one can describe weak localization effect by classical Drude-Boltzmann equation with the renormalized differential cross-section proportional to the Cooperon.

Let us now demonstrate that a similar description is applicable to our problem. To this end, we first consider transport in our setup within the classical approximation, which implies that the magnetic impurity is described by the forward and backward scattering probabilities:

$$t_{\rm f}^0 = \cos^2\theta, \qquad t_{\rm b}^0 = \sin^2\theta. \qquad (21)$$

The classical transmission coefficient can be presented as the sum over contributions from classical trajectories propagating clockwise and counterclockwise, and having winding index n:

$$\mathcal{T}_{\rm cl} = \frac{r^4}{2}\sum_{n=0}\left[J_1^{(n)} + J_2^{(n)}\right]. \qquad (22)$$

Having in mind that the impurity is placed in the upper shoulder of the interferometer (see Fig. 1), one can easily find the following set of the recurrent equations for classical currents $J_{1,2}^{(n)}$:

$$\begin{aligned} J_1^{(n+1)} &= J_1^{(n)} t^4\cos^2\theta + J_2^{(n)} t^2\sin^2\theta, \\ J_2^{(n+1)} &= J_1^{(n)} t^6\sin^2\theta + J_2^{(n)} t^4\cos^2\theta, \end{aligned} \qquad (23)$$

with $J_1^{(0)} = \cos^2\theta$ and $J_2^{(0)} = 1 + t^2\sin^2\theta$. Solving these equations and expressing r and t via γ [see Eq. (4)], we find

$$\mathcal{T}_{\rm cl} = 2\gamma\frac{4\gamma + (\gamma^2 - 4\gamma + 1)\sin^2\theta}{4\gamma(1+\gamma^2) + (1-\gamma)^4\sin^2\theta}. \qquad (24)$$

This equation is simplified for $\theta \to 0$:

$$\mathcal{T}_{\rm cl} \approx \frac{2\gamma}{1+\gamma^2} - \frac{2\gamma^2\theta^2}{(1+\gamma^2)^2}, \qquad (25)$$

and even more so when $\gamma \to 0$:

$$\mathcal{T}_{\rm cl} \approx 2\gamma - 2\gamma^2\theta^2. \qquad (26)$$

Equation (24) does not contain contribution from interfering trajectories and, hence, is flux-independent. It can be obtained from exact equation for quantum transmission coefficient by averaging over the flux

$$\mathcal{T}_{\rm cl} = \langle\mathcal{T}\rangle_\phi. \qquad (27)$$

In particular, one can check that Eq. (25) is obtained by averaging of Eq. (14) over ϕ.

Next, we obtain Eq. (14) in a different way by calculating quantum corrections to the classical scattering probabilities $t_{\rm f}^0$ and $t_{\rm b}^0$. The latter describe single scattering processes by magnetic impurity shown in the left panels of Figs. 6 (a) and (b), respectively. Let us consider two processes involving multiple scattering by magnetic impurity after some number of ballistic returns. First process is shown in Fig. 6a (right panel) and describes the first order quantum correction to $t_{\rm f}^0$. The first order correction to the probability of the backward scattering is shown in the right panel of Fig. 6 (b). Both processes involve ballistic returns to the magnetic impurity after a number of revolutions around the ring in which the electron wave splits into two parts passing the setup in the opposite directions with equal winding numbers. Summing over winding numbers, we find "ballistic Cooperon"

$$\mathcal{C} = \frac{t^4 e^{4i\pi\phi}}{1 - t^4\cos^2\theta e^{4i\pi\phi}} + \frac{t^4 e^{-4i\pi\phi}}{1 - t^4\cos^2\theta e^{-4i\pi\phi}}, \qquad (28)$$

which represents the contribution of the processes shown in Fig 6(c). Notice that

$$\langle\mathcal{C}\rangle_\phi = 0\,. \qquad (29)$$

One can easily calculate contributions from these processes to scattering probabilities

$$\delta t_{\rm f} = -\cos^2\theta\sin^2\theta\;\mathcal{C}, \quad \delta t_{\rm b} = \cos^2\theta\sin^2\theta\;\mathcal{C}. \qquad (30)$$

As seen, these equations obey probability conservation law:

$$\delta t_{\rm f} + \delta t_{\rm b} = 0. \qquad (31)$$

The total scattering probabilities incorporating first order quantum corrections read

$$t_{\rm f} = t_{\rm f}^0 + \delta t_{\rm f}, \quad t_{\rm b} = t_{\rm b}^0 + \delta t_{\rm b}. \qquad (32)$$

Let us now consider a limit of small θ. In this case, only first order corrections, containing single Cooperon, contribute. Also, one can calculate $\mathcal{C}$ in this limit for $\theta = 0$. Then, from Eqs. (28) and (4) we find

$$\delta t_{\rm b} \approx \theta^2\mathcal{C}|_{\theta=0}. \qquad (33)$$

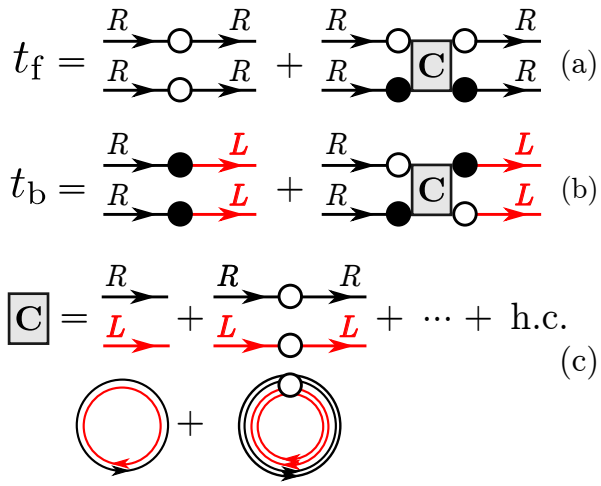

FIG. 6: Forward (a) and backward (b) single scattering events [left panels of (a) and (b), respectively] and coherent scattering processes [right panels of (a) and (b)] leading to enhancement of scattering probabilities due to ballistic returns to the magnetic impurity. Probabilities of both coherent processes are proportional to the ballistic Cooperon (c) which is given by the sum over closed ballistic loops formed by trajectories propagating in the opposite directions and having different winding numbers. Open circles and black dots describe amplitudes of single forward and backward scattering events, respectively. The contributions of coherent processes [right (a) and (b) panels] coincide by absolute value, while the phase factor i arising in each backscattering act enters in different way, $\delta t_{\rm f} = \cos^2\theta(-i\sin\theta)^2 C$, $\delta t_{\rm b} = \cos^2\theta(i\sin\theta)(-i\sin\theta)C$, which ensures the probability conservation: $\delta t_{\rm f} + \delta t_{\rm b} = 0$.

Since $t_{\rm b}^0 \simeq \theta^2$ at small θ, see Eq. (21), the total factor appearing due to the coherent scattering is given by

$$\frac{t_{\rm b}}{t_{\rm b}^0} \approx 1 + \mathcal{C}|_{\theta=0} = \frac{8\gamma(1+\gamma^2)^2 A_\gamma}{32\gamma^2 B_\gamma + 1 - \cos(4\pi\phi)}, \tag{34}$$

where A_γ is given by Eq. (15). For $\gamma \ll 1$, this equation becomes

$$\frac{t_{\rm b}}{t_{\rm b}^0} \approx \frac{8\gamma}{32\gamma^2 + 1 - \cos(4\pi\phi)}. \tag{35}$$

Exactly at the resonances, the backscattering probability is enhanced by the large factor

$$\left(\frac{t_{\rm b}}{t_{\rm b}^0}\right)_{\rm max} = \frac{1}{4\gamma} \gg 1, \tag{36}$$

as compared to the classical backward probability. On the other hand, the classical backscattering probability is suppressed beyond the resonance region. The dependence $t_{\rm b}(\phi)$ is shown in Fig. 7.

The dependence of $\mathcal{T}$ on ϕ at $\theta \to 0$ is obtained by replacing θ^2 in $\mathcal{T}_{cl}$, Eq. (25), by $\theta^2\left(t_{\rm b}/t_{\rm b}^0\right) = \theta^2(1+\mathcal{C}|_{\theta=0})$; the relation (27) is fulfilled due to (29).

Concluding here, we observe that the effective backward scattering is dramatically enhanced in vicinity of integer and half-integer values of the magnetic flux and is suppressed at other values of the flux.

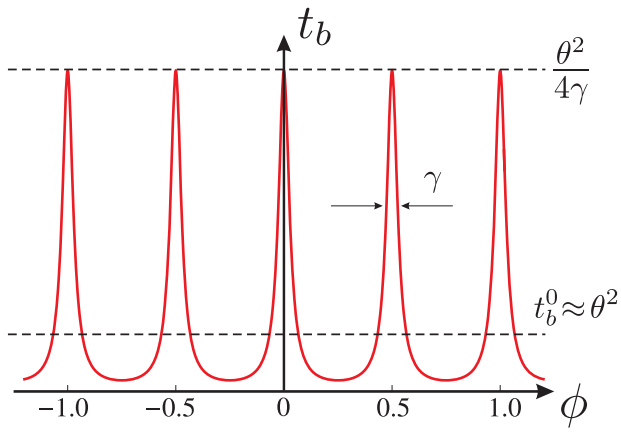

FIG. 7: Dependence of total backscattering probability $t_{\rm b}$ on magnetic flux for weak tunneling coupling ($\gamma \ll 1$). This probability is strongly enhanced in the vicinity of the resonances and suppressed outside resonance region as compared to the classical flux-independent probability $t_{\rm b}^0$ shown by dashed line.

VI. DEPHASING INDUCED BY DYNAMICS OF MAGNETIC IMPURITY

One of the key problems related to efficiency of any interferometer is the dephasing caused by inelastic processes. Here we briefly discuss one of the possible mechanisms of dephasing. A more detailed analysis will be presented elsewhere [98].

The dominating mechanism of dephasing in low dimensional systems is usually connected with the electron-electron interaction. For tunneling AB interferometers made of conventional (non-helical) single-channel ballistic wires, the effect of interaction for $T \gg \Delta$ was studied in Ref. [68] (see also Ref. [72]). It was found that antiresonances in the dependence $G(\phi)$ split into a series of narrow peaks separated by distance α with a smooth envelope of the width $\alpha\sqrt{T/\Delta}$, where α is the dimensionless interaction constant. Each peak is broadened by dephasing within the width $\gamma T/\Delta$, which turns out to be interaction-independent and gets suppressed with closing the interferometer ($\gamma \to 0$). The underlying physics is related to interaction of the tunneling electrons with so-called zero-mode fluctuations, i.e. tunneling-induced fluctuations of total numbers of right- and left-moving electrons, N_R and N_L, respectively.

Similar dephasing would also occur in the case under discussion [104]. There is however, a competing contribution to dephasing caused by chaotic dynamics of impurity moment $\mathbf{M}$. The latter mechanism can be more effective in an almost closed interferometer of sufficiently large size L. The random behavior of $\mathbf{M}(t)$ can occur for a number of reasons. First of all, the dynamics of $\mathbf{M}(t)$ appears due to the exchange interaction with the thermal bath of electrons in the helical edge modes. This mechanism

was recently discussed in Refs. [42] (see also [105, 106]) for the case of infinite edge, where a general equation for relaxation of averaged moment $\langle \mathbf{M}(t)\rangle$ was derived. Simple estimates show that for a ring-shaped edge of finite length L weakly coupled to thermalized leads the theory developed in [42] should be essentially modified. Most importantly, zero mode fluctuations come into play and dramatically change the dephasing action in close analogy with the effect of the electron-electron interaction [68]. This would lead to a non-trivial dynamics of $\mathbf{M}(t)$.

Here, we confine ourselves to the analysis of much simpler mechanism, namely, we assume that a slow random dynamics of $\mathbf{M}(t)$ is caused by the interaction with external magnetic bath, in particular, with thermal bath of bulk magnetic impurities. We also assume that this bath is isotropic, so that the correlation function describing the magnetic moment relaxation is given by

$$\langle M_\alpha(0)M_\beta(t)\rangle = \frac{M^2}{3}\delta_{\alpha\beta}e^{-\Gamma t}, \tag{37}$$

where Γ is the isotropic relaxation rate.

The dephasing rate caused by relaxation (37) can be calculated as follows. We assume that the electron spin at the position of the magnetic impurity is directed along the $\hat{z}$ axis, and the components of the classical vector $\mathbf{M}$ are given by: $M_z = M\cos\chi, M_x = M\sin\chi\cos\varphi, M_y = M\sin\chi\sin\varphi$. A slow evolution of $\mathbf{M}(t)$ is encoded in the time dependence of angles $\chi = \chi(t)$ and $\varphi = \varphi(t)$. For fixed values of χ and φ the scattering matrix $\hat{S}_M$ is given by Eq. (7) with $\theta = gM\sin\chi$, where $g \ll 1$ is the exchange coupling constant. Let us discuss the simplest situation, when the scattering on magnetic impurity is considered in the lowest order with respect to θ, whereas χ is arbitrary. The correction to the backscattering for static impurity is given in this case by Eq. (33). In order to take into account the slow dynamics of $\mathbf{M}$ this equation should be modified as follows:

$$\delta t_{\rm b} = 2{\rm Re}\sum_{n=0}^{\infty}\left(t^4 e^{4i\pi\phi}\right)^{n+1}\left\langle\theta(0)\theta(t_n)e^{i(\varphi(0)-\varphi(t_n))}\right\rangle, \tag{38}$$

where $t_n = 2\pi n/\Delta$. Next, we notice that $\left\langle\theta(0)\theta(t_n)e^{i(\varphi(0)-\varphi(t_n)}\right\rangle = g^2\langle M_+(0)M_-(t)\rangle$ (with $M_\pm = M_x \pm iM_y$) and use Eq. (37). For $\Gamma \ll \Delta$ and $\gamma \ll 1$, we find that Eq. (14) becomes

$$\mathcal{T} \approx 2\gamma - \frac{16\gamma^3\langle\theta^2\rangle}{1-\cos(4\pi\phi)+32(\gamma+\gamma_\varphi)^2}, \tag{39}$$

where

$$\gamma_\varphi = \frac{\pi\Gamma}{4\Delta} \tag{40}$$

is the dimensionless dephasing rate and $\langle\theta^2\rangle = g^2M^2\langle\sin^2\chi\rangle = 2g^2M^2/3$. The dephasing given by Eq. (40) should dominate over interaction-induced one provided that relaxation rate Γ is large as compared to interaction-induced splitting of antiresonances: $\Gamma \gg \alpha\sqrt{T\Delta}$.

VII. CONCLUSIONS

In this paper we studied the transport through the Aharonov-Bohm interferometer formed by helical edge states which are tunnel-coupled to metallic leads in the presence of a magnetic impurity. We demonstrated that at relatively high temperatures, $T \gg \Delta$, (which, for typical values of parameters, corresponds to temperatures higher than several kelvins) the tunneling conductance of the interferometer shows sharp antiresonances The antiresonances are separated by distance $\Delta\phi = 1/2$, which means that the tunneling conductance is periodic function of the magnetic flux with the period given by half of the flux quantum. We interpret the resonance behavior as a coherent enhancement of backward scattering off magnetic impurity at integer and half-integer values of flux, which is accompanied by suppression of the effective scattering at other values of flux. Both enhancement and suppression are due to the interference of processes involving multiple returns (clockwise and counterclockwise) to magnetic impurity after revolutions around interferometer circumference — the phenomenon similar to weak-localization-induced enhancement of backscattering. We demonstrate that the quantum correction to the tunneling conductance is proportional to flux-dependent "ballistic Cooperon". A very sharp dependence of the conductance is very promising in view of possible applications in the area of extremely sensitive detectors of magnetic fields. Most importantly, the predicted dependence of the effective scattering probability on the magnetic flux allows for flux-tunable control of the magnetic disorder.

VIII. ACKNOWLEDGEMENTS

The work of R.N. and V.K. was supported by the joint grant of the Russian Science Foundation (Grant No. 16-42-01035) and the Deutsche Forschungsgemeinschaft (Grant No. MI 658-9/1).

Appendix A: Temperature averaging

In this Appendix, we present the equations for the energy averaging within the temperature window. The energy dependence appears in the transmission amplitudes via the factor $\exp(ikL)$. Due to the condition $T \gg \Delta$, this exponent rapidly oscillates when energy changes within the temperature window around the Fermi energy. To the exponential precision, one can thus replace the energy averaging by the averaging over the phase $\varphi = kL$ within the interval $0 < \varphi < 2\pi$. Next one can replace $\exp(i\varphi) = z$ and reduce the averaging over φ to the calculation of contour integral over z. In all considered cases the integrand in appearing integrals has a simple pole structure and can be easily evaluated.

In particular, for any a such that $|a| < 1$ and any analytical function $F(z)$, we have

$$\left\langle \frac{F\left(e^{i\varphi}\right)}{1-ae^{-i\varphi}} \right\rangle_{\varphi} = F(a), \tag{A1}$$

Using this equation, we find for any b ($|b| < 1$) and c ($|c| < 1$):

$$\left\langle \frac{e^{in\varphi}}{(1-ae^{-i\varphi})\,(1-be^{i\varphi})\,(1-ce^{i\varphi})} \right\rangle_{\varphi} = \frac{a^n}{(1-ba)(1-ca)}\,, \tag{A2}$$

and

$$\left\langle \left|\frac{1}{1-ae^{-i\varphi}}\right|^2 \left|\frac{1}{1-be^{-i\varphi}}\right|^2 \right\rangle_{\varphi} = \frac{1-|a|^2|b|^2}{(1-|a|^2)(1-|b|^2)|1-b^*a|^2}\,. \tag{A3}$$

Appendix B: Non-perturbative analysis

In order to calculate the conductance for arbitrary relation between θ, γ and $\delta\phi$ (all these parameters are assumed to be small as compared to unity) one can use an approach developed in [70, 96] for conventional (non-helical) interferometers. For simplicity, we only consider the case of the interferometer with equal shoulders: $L_1 = L_2$.

The electron tunneling transmission amplitude is a matrix $\hat{t} = \hat{t}(\epsilon)$ in a spin space with elements $t_{\alpha\beta} = \langle\alpha|t|\beta\rangle$. The transmission coefficient is expressed in terms of this amplitude as follows:

$$\mathcal{T}(\epsilon) = \frac{1}{2}\mathrm{Tr}\ \hat{t}\hat{t}^{\dagger}. \tag{B1}$$

The tunneling trajectory with n full revolutions around the setup has a length $L_n = L(n+1/2)$. The transmission amplitude can be expressed as a sum over n:

$$\hat{t}(\epsilon) = \sum_{n=0}^{\infty} \hat{\beta}_n e^{ikL_n}. \tag{B2}$$

The quantity $\hat{\beta}_n$ consists of two contributions: trajectories ending at the bottom semicircle, $\hat{\beta}_n^+$ and at the top semicircle, $\hat{\beta}_n^-$. The vector constructed out of these two contributions,

$$\vec{\hat{\beta}}_n = \begin{pmatrix} \hat{\beta}_n^+ \\ \hat{\beta}_n^- \end{pmatrix}, \tag{B3}$$

obeys a recurrence relation

$$\vec{\hat{\beta}}_{n+1} = \hat{A}\vec{\hat{\beta}}_n,$$

where $\hat{A}$ is certain $n-$independent matrix. Then, $\vec{\hat{\beta}}_n$ is given by $\hat{\beta}_n = \vec{e}\hat{A}^n\vec{\hat{\beta}}_0$, where

$$\vec{e} = \begin{pmatrix} \mathbf{1} \\ \mathbf{1} \end{pmatrix}. \tag{B4}$$

The transmission coefficient,

$$\mathcal{T}(\epsilon) = \frac{1}{2}\mathrm{Tr}\sum_{n,m=0}^{\infty} \hat{\beta}_n\hat{\beta}_m^{\dagger} e^{ik(L_n-L_m)}, \tag{B5}$$

after energy averaging under condition $T \gg \Delta$ has only nonzero terms with $n = m$ and is expressed in terms of matrix $\hat{A}$ as follows

$$\mathcal{T}(\phi) = \frac{1}{2}\mathrm{Tr}\sum_{n=0}^{\infty} |\hat{\beta}_n|^2 = \frac{1}{2}\mathrm{Tr}\sum_{n=0}^{\infty} |\vec{e}\hat{A}^n\vec{\hat{\beta}}_0|^2. \tag{B6}$$

Calculation of the sum (see technical details in Refs. [70, 96]) yields a matrix $\hat{B} = (\mathbf{1} - \hat{A}\otimes\hat{A}^{\dagger})^{-1}$ acting in the space of doubled dimension. Hence, the problem is reduced to a straightforward (albeit cumbersome) calculation of matrix elements of $\hat{B}$.

Because of the helical nature of the edge state the matrix $\hat{A}$ is simplified since we assume that counterclockwise electron propagation mode with the spin up as well as clockwise mode with spin down are absent:

$$\hat{A} = \begin{pmatrix} 0 & 0 & 0 & 0 \\ 0 & -e^{2i\pi\phi}t^2\cos\theta & -e^{2iks}t^3\sin\theta & 0 \\ 0 & e^{-2iks}t\sin\theta & -e^{-2i\pi\phi}t^2\cos\theta & 0 \\ 0 & 0 & 0 & 0 \end{pmatrix}. \tag{B7}$$

The initial amplitudes read

$$\hat{\beta}_0^+ = \begin{pmatrix} 0 & 0 \\ -e^{i\pi\phi}(1-t^2) & -e^{2iks+i\pi\phi}t(1-t^2)\sin\theta \end{pmatrix}, \quad \hat{\beta}_0^- = \begin{pmatrix} 0 & -e^{-i\pi\phi}(1-t^2)\cos\theta \\ 0 & 0 \end{pmatrix}. \tag{B8}$$

Using these formula, one can represent the transmission coefficient as a ratio of two rather cumbersome functions of θ, γ and $\delta\phi$. In the limit $\theta, \gamma, \delta\phi \ll 1$, one can expand both functions over θ, γ and $\delta\phi$ up to the terms of second order. Doing so, we arrive at Eq. (18) of the main text. One can show that this equation is also valid for $L_1 \neq L_2$.

[1] Y. Aharonov and D. Bohm, Phys. Rev. **115**, 485 (1959).

[2] A. G. Aronov and Y. V. Sharvin, Rev. Mod. Phys. **59**,

755 (1987).
[3] C. L. Kane and E. J. Mele, Phys. Rev. Lett. **95**, 226801 (2005).
[4] C. L. Kane and E. J. Mele, Phys. Rev. Lett. **95**, 146802 (2005).
[5] B. A. Bernevig, T. L. Hughes, and S.-C. Zhang, Science **314**, 1757 (2006).
[6] M. König, S. Wiedmann, C. Brune, A. Roth, H. Buhmann, L. W. Molenkamp, X.-L. Qi, and S.-C. Zhang, Science **318**, 766 (2007).
[7] A. Roth, C. Brüne, H. Buhmann, L. W. Molenkamp, J. Maciejko, X.-L. Qi, S.-C. Zhang, Science **325**, 294 (2009).
[8] G. M. Gusev, Z. D. Kvon, O. A. Shegai, N. N. Mikhailov, S. A. Dvoretsky, J. C. Portal, Phys. Rev. B **84**, 121302(R) (2011).
[9] C. Brüne, A. Roth, H. Buhmann, E. M. Hankiewicz, L. W. Molenkamp, J. Maciejko, X.-L. Qi, S.-C. Zhang, Nature Phys. 8, 485 (2012).
[10] A. Kononov, S. V. Egorov, Z. D. Kvon, N. N. Mikhailov, S. A. Dvoretsky, E. V. Deviatov, JETP Lett. **101**, 814 (2015).
[11] M. Z. Hasan and C. L. Kane, Rev. Mod. Phys. **82**, 3045 (2010).
[12] Xiao-Liang Qi and Shou-Cheng Zhang, Rev. Mod. Phys. **83**, 1057 (2011).
[13] R.-L. Chu, J. Li, J. K. Jain, and S.-Q. Shen, Phys. Rev. B **80**, 081102 (2009).
[14] D. Hsieh, Y. Xia, D. Qian, L. Wray, J. H. Dil, F. Meier, J. Osterwalder, L. Patthey, J. G. Checkelsky, N. P. Ong, et al., Nature **460**, 1101 (2009).
[15] J. H. Bardarson, P. W. Brouwer, and J. E. Moore, Phys. Rev. Lett. **105**, 156803 (2010).
[16] H. Peng, K. Lai, D. Kong, S. Meister, Y. Chen, X.-L. Qi, S.-C. Zhang, Z.-X. Shen, and Y. Cui, Nat Mater **9**, 225 (2010).
[17] P. Michetti and P. Recher, Phys. Rev. B **83**, 125420 (2011).
[18] P. Delplace, J. Li, and M. Büttiker, Phys. Rev. Lett. **109**, 246803 (2012).
[19] S. Masuda and Y. Kuramoto, Phys. Rev. B **85**, 195327 (2012).
[20] J. H. Bardarson and J. E. Moore, Reports on Progress in Physics **76**, 056501 (2013).
[21] N. Kainaris, I. V. Gornyi, S. T. Carr, and A. D. Mirlin, Phys. Rev. B **90**, 075118 (2014).
[22] G. M. Gusev, Z. D. Kvon, E. B. Olshanetsky, A. D. Levin, Y. Krupko, J. C. Portal, N. N. Mikhailov, and S. A. Dvoretsky, Phys. Rev. B **89**, 125305 (2014).
[23] E. B. Olshanetsky, Z. D. Kvon, G. M. Gusev, A. D. Levin, O. E. Raichev, N. N. Mikhailov, and S. A. Dvoretsky, Phys. Rev. Lett. **114**, 126802 (2015).
[24] P. Dutta, A. Saha, and A. M. Jayannavar, Physical Review B **94**, 195414 (2016).
[25] L. A. Jauregui, M. T. Pettes, L. P. Rokhinson, L. Shi, and Y. P. Chen, Nat Nano **11**, 345 (2016).
[26] B.-C. Lin, S. Wang, L.-X. Wang, C.-Z. Li, J.-G. Li, D. Yu, and Z.-M. Liao, Phys. Rev. B **95**, 235436 (2017).
[27] N. Kainaris, I. V. Gornyi, A. Levchenko, and D. G. Polyakov, Phys. Rev. B **95**, 045150 (2017).
[28] G.M. Gusev, Z.D. Kvon, O.A. Shegai, N.N. Mikhailov, S.A. Dvoretsky, Solid.State Commun. **205**, 4 (2015).
[29] L. Du, I. Knez, G. Sullivan, and R.-R. Du, Phys. Rev. Lett. **114**, 096802 (2015).
[30] S.-B. Zhang, Y.-Y. Zhang, and S.-Q. Shen, Phys. Rev. B **90**, 115305 (2014).
[31] L.-H. Hu, D.-H. Xu, F.-C. Zhang, and Y. Zhou, Phys. Rev. B **94**, 085306 (2016).
[32] J. Maciejko, Ch. Liu, Y. Oreg, X.-L. Qi, C. Wu, S.- C. Zhang, Phys. Rev. Lett. **102**, 256803 (2009).
[33] Y. Tanaka, A. Furusaki, K. A. Matveev, Phys. Rev. Lett. **106**, 236402 (2011).
[34] F. Dolcini, Phys. Rev. B **83**, 165304 (2011).
[35] J. I. Väyrynen, M. Goldstein, L. I. Glazman, Phys. Rev. Lett. **110**, 216402 (2013).
[36] J. I. Väyrynen, M. Goldstein, Y. Gefen, L. I. Glazman, Phys. Rev. B **90**, 115309 (2014).
[37] B. L. Altshuler, I. L. Aleiner, V. I. Yudson, Phys. Rev. Lett. **111**, 086401 (2013).
[38] V. Cheianov and L. I. Glazman, Phys. Rev. Lett. **110**, 206803 (2013).
[39] O. M. Yevtushenko, A. Wugalter, V. I. Yudson, B. L. Altshuler, Europhysics Letters, **112**, 57003 (2015).
[40] L. Kimme, B. Rosenow, A. Brataas, Phys. Rev. B **93**, 081301 (2016).
[41] J. I. Väyrynen, F. Geissler, L. I. Glazman, Phys. Rev. B **93**, 241301(R) (2016).
[42] P. D. Kurilovich, V. D. Kurilovich, I. S. Burmistrov, M. Goldstein, arXiv:1710.00384, unpublished
[43] M. Büttiker, Y. Imry, and M. Y. Azbel, Phys. Rev. A **30**, 1982 (1984).
[44] Y. Gefen, Y. Imry, and M. Y. Azbel, Phys. Rev. Lett. **52**, 129 (1984).
[45] M. Büttiker, Y. Imry, R. Landauer, and S. Pinhas, Phys. Rev. B **31**, 6207 (1985).
[46] E. A. Jagla and C. A. Balseiro, Phys. Rev. Lett. **70**, 639 (1993).
[47] A. Yacoby, M. Heiblum, V. Umansky, H. Shtrikman, and D. Mahalu, Phys. Rev. Lett. **73**, 3149 (1994).
[48] A. Yacoby, M. Heiblum, D. Mahalu, and H. Shtrikman, Phys. Rev. Lett. **74**, 4047 (1995).
[49] A. Yacoby, R. Schuster, and M. Heiblum, Phys. Rev. B **53**, 9583 (1996).
[50] R. Schuster, E. Buks, M. Heiblum, D. Mahalu, V. Umansky, and H. Shtrikman, Nature **385**, 417 (1997).
[51] E. Buks, R. Schuster, M. Heiblum, D. Mahalu, and V. Umansky, Nature **391**, 871 (1998).
[52] J. M. Kinaret, M. Jonson, R. I. Shekhter, and S. Eggert, Phys. Rev. B **57**, 3777 (1998).
[53] A. van Oudenaarden, M. H. Devoret, Y. V. Nazarov, and J. E. Mooij, Nature **391**, 768 (1998).
[54] A. A. Bykov, A. K. Bakarov, L. V. Litvin, and A. I. Toropov, Journal of Experimental and Theoretical Physics Letters **72**, 209 (2000).
[55] A. A. Bykov, D. G. Baksheev, L. V. Litvin, V. P. Migal', E. B. Ol'shanetskii, M. Cassé, D. K. Maude, and J. C. Portal, Journal of Experimental and Theoretical Physics Letters **71**, 434 (2000).
[56] O. M. Auslaender, A. Yacoby, R. de Picciotto, K. W. Baldwin, L. N. Pfeiffer, and K. W. West, Science **295**, 825 (2002).
[57] Y. Ji, Y. Chung, D. Sprinzak, M. Heiblum, D. Mahalu, and H. Shtrikman, Nature **422**, 415 (2003).
[58] P. Samuelsson, E. V. Sukhorukov, and M. Büttiker, Phys. Rev. Lett. **92**, 026805 (2004).
[59] M. Avinun-Kalish, M. Heiblum, O. Zarchin, D. Mahalu, and V. Umansky, Nature **436**, 529 (2005).

[60] I. Neder, M. Heiblum, Y. Levinson, D. Mahalu, and V. Umansky, Phys. Rev. Lett. **96**, 016804 (2006).
[61] I. Neder, N. Ofek, Y. Chung, M. Heiblum, D. Mahalu, and V. Umansky, Nature **448**, 333 (2007).
[62] I. Neder, M. Heiblum, D. Mahalu, and V. Umansky, Phys. Rev. Lett. **98**, 036803 (2007).
[63] P. Roulleau, F. Portier, D. C. Glattli, P. Roche, A. Cavanna, G. Faini, U. Gennser, and D. Mailly, Phys. Rev. B **76**, 161309 (2007).
[64] P. Roulleau, F. Portier, P. Roche, A. Cavanna, G. Faini, U. Gennser, and D. Mailly, Phys. Rev. Lett. **100**, 126802 (2008).
[65] D.-I. Chang, G. L. Khym, K. Kang, Y. Chung, H.-J. Lee, M. Seo, M. Heiblum, D. Mahalu, and V. Umansky, Nature Physics **4**, 205 (2008).
[66] Y. Zhang, D. T. McClure, E. M. Levenson-Falk, C. M. Marcus, L. N. Pfeiffer, and K. W. West, Phys. Rev. B **79**, 241304 (2009).
[67] N. Ofek, A. Bid, M. Heiblum, A. Stern, V. Umansky, and D. Mahalu, Proceedings of the National Academy of Sciences **107**, 5276 (2010).
[68] A. P. Dmitriev, I. V. Gornyi, V. Y. Kachorovskii, and D. G. Polyakov, Phys. Rev. Lett. **105**, 036402 (2010).
[69] E. Weisz, H. K. Choi, M. Heiblum, Y. Gefen, V. Umansky, and D. Mahalu, Phys. Rev. Lett. **109**, 250401 (2012).
[70] P. M. Shmakov, A. P. Dmitriev, and V. Y. Kachorovskii, Phys. Rev. B **87**, 235417 (2013).
[71] A. P. Dmitriev, I. V. Gornyi, V. Y. Kachorovskii, D. G. Polyakov, and P. M. Shmakov, JETP Letters **100**, 839 (2015).
[72] A. P. Dmitriev, I. V. Gornyi, V. Y. Kachorovskii, and D. G. Polyakov, Phys. Rev. B **96**, 115417 (2017).
[73] Y. Aharonov and A. Casher, Phys. Rev. Lett. **53**, 319 (1984).
[74] H. Mathur and A. D. Stone, Phys. Rev. B **44**, 10957 (1991).
[75] H. Mathur and A. D. Stone, Phys. Rev. Lett. **68**, 2964 (1992).
[76] A. G. Aronov and Y. B. Lyanda-Geller, Phys. Rev. Lett. **70**, 343 (1993).
[77] T.-Z. Qian and Z.-B. Su, Phys. Rev. Lett. **72**, 2311 (1994).
[78] J. Nitta, F. E. Meijer, and H. Takayanagi, Applied Physics Letters **75**, 695 (1999).
[79] D. Frustaglia and K. Richter, Phys. Rev. B **69**, 235310 (2004).
[80] B. Molnár, F. M. Peeters, and P. Vasilopoulos, Phys. Rev. B **69**, 155335 (2004).
[81] U. Aeberhard, K. Wakabayashi, and M. Sigrist, Phys. Rev. B **72**, 075328 (2005).
[82] R. Citro and F. Romeo, Phys. Rev. B **73**, 233304 (2006).
[83] M. Pletyukhov, V. Gritsev, and N. Pauget, Phys. Rev. B **74**, 045301 (2006).
[84] R. Citro, F. Romeo, and M. Marinaro, Phys. Rev. B **74**, 115329 (2006).
[85] A. A. Kovalev, M. F. Borunda, T. Jungwirth, L. W. Molenkamp, and J. Sinova, Phys. Rev. B **76**, 125307 (2007).
[86] F. Romeo, R. Citro, and M. Marinaro, Phys. Rev. B **78**, 245309 (2008).
[87] A. M. Lobos and A. A. Aligia, Phys. Rev. Lett. **100**, 016803 (2008).
[88] M. Pletyukhov and U. Zülicke, Phys. Rev. B **77**, 193304 (2008).
[89] V. Moldoveanu and B. Tanatar, Phys. Rev. B **81**, 035326 (2010).
[90] A. Aharony, Y. Tokura, G. Z. Cohen, O. Entin-Wohlman, and S. Katsumoto, Phys. Rev. B **84**, 035323 (2011).
[91] P. Michetti and P. Recher, Phys. Rev. B **83**, 125420 (2011).
[92] M. König, A. Tschetschetkin, E. M. Hankiewicz, J. Sinova, V. Hock, V. Daumer, M. Schäfer, C. R. Becker, H. Buhmann, and L. W. Molenkamp, Phys. Rev. Lett. **96**, 076804 (2006).
[93] T. Bergsten, T. Kobayashi, Y. Sekine, and J. Nitta, Phys. Rev. Lett. **97**, 196803 (2006).
[94] F. Nagasawa, J. Takagi, Y. Kunihashi, M. Kohda, and J. Nitta, Phys. Rev. Lett. **108**, 086801 (2012).
[95] F. Nagasawa, D. Frustaglia, H. Saarikoski, K. Richter, and J. Nitta, Nature Communications **4**, 2526 (2013).
[96] P. M. Shmakov, A. P. Dmitriev, and V. Y. Kachorovskii, Physical Review B **85**, 075422 (2012).
[97] See Appendix in A.P. Dmitriev, I.V. Gornyi, V.Yu. Kachorovskii, and D.G. Polyakov, arXiv:0911.0911.
[98] R. A. Niyazov, D. N. Aristov, and V. Y. Kachorovskii, to be published.
[99] D. N. Aristov and R. A. Niyazov, Phys. Rev. B **94**, 035429 (2016).
[100] D. N. Aristov, A.P. Dmitriev, I.V. Gornyi, V.Yu. Kachorovskii, D. G. Polyakov, and P. Wölfle, Phys. Rev. Lett. 105, 266404 (2010).
[101] M. V. Berry, Proceedings of the Royal Society A: Mathematical, Physical and Engineering Sciences **392**, 45 (1984).
[102] S. Chakravarty and A. Schmid, Physics Reports **140**, 193 (1986).
[103] A. P. Dmitriev, V. Y. Kachorovskii, and I. V. Gornyi, Phys. Rev. B **56**, 9910 (1997).
[104] An important modification of results of Ref. [68] in the case of helical ring coupled to magnetic impurity is related to the fact that N_R and N_L are non conserved even in the fully closed setup ($\gamma = 0$) because of the impurity-induced backscattering.
[105] P. D. Kurilovich, V. D. Kurilovich, I. S. Burmistrov, Phys. Rev. B **94**, 155408 (2016).
[106] V. D. Kurilovich, P. D. Kurilovich, I. S. Burmistrov, Phys. Rev. B **95**, 115430 (2017).